

Supporting Information:

Correlated Topological States in Graphene Nanoribbon Heterostructures

Jan-Philip Joost,[†] Antti-Pekka Jauho,[‡] and Michael Bonitz^{*,†}

[†]*Institut für Theoretische Physik und Astrophysik, Christian-Albrechts-Universität zu Kiel,*

D-24098 Kiel, Germany

[‡]*CNG, DTU Physics, Technical University of Denmark*

E-mail: bonitz@theo-physik.uni-kiel.de

Phone: +49 (0)431 880-4122. Fax: +49 (0)431 880-4094

Green function theory

Despite the fully diagonal interaction the exact solution of the Hubbard Hamiltonian [cf. Eq. (1) in the main text] is known only in some limiting cases¹ and for small one-dimensional systems.² For large two-dimensional lattices an approximate solution of the Hubbard model can be found using the Green functions approach.

The retarded (R) and advanced (A) components of the single-particle Green function obey the Dyson equation [cf. Eq. (2) in the main text]

$$\mathbf{G}^{\text{R/A}}(\omega) = \mathbf{G}_0^{\text{R/A}}(\omega) + \mathbf{G}_0^{\text{R/A}}(\omega) \boldsymbol{\Sigma}^{\text{R/A}}(\omega) \mathbf{G}^{\text{R/A}}(\omega), \quad (1)$$

where all quantities are matrices in the orthonormal basis $|i\rangle$ defined by the $2p_z$ atomic orbitals of the carbon atoms that make up the GNR heterostructure. If the exact self-energy

$\Sigma^{\text{R/A}}(\omega)$ of the system was known, Eq. 1 would provide the exact single-particle Green function. However, in practice many-body approximations to the self-energy have to be used. The uncorrelated Green function is given by

$$G_{0,ij}^{\text{R/A}}(\omega) = \langle i | (\omega - \hat{h} \pm i\eta)^{-1} | j \rangle, \quad \eta \rightarrow 0 \quad (2)$$

and depends only on the single-particle Hamiltonian

$$\hat{h} = -J \sum_{\langle i,j \rangle, \alpha} \hat{c}_{i\alpha}^\dagger \hat{c}_{j\alpha}, \quad (3)$$

where J is the hopping amplitude between adjacent lattice sites, and the operators $\hat{c}_{i\alpha}^\dagger$ and $\hat{c}_{j\alpha}$ create and annihilate an electron with spin projection α at site i and j , respectively. For the correlated Green function the lesser ($<$) and greater ($>$) components can be determined by

$$\mathbf{G}^<(\omega) = -f_{\text{F}}(\omega - \mu) [\mathbf{G}^{\text{R}}(\omega) - \mathbf{G}^{\text{A}}(\omega)], \quad (4)$$

$$\mathbf{G}^>(\omega) = \bar{f}_{\text{F}}(\omega - \mu) [\mathbf{G}^{\text{R}}(\omega) - \mathbf{G}^{\text{A}}(\omega)], \quad (5)$$

with the Fermi function $f_{\text{F}}(\omega) = 1/(e^{\beta\omega} + 1)$, $\bar{f}_{\text{F}}(\omega) = 1 - f_{\text{F}}(\omega)$, and $\mathbf{G}^{\text{A}}(\omega) = [\mathbf{G}^{\text{R}}(\omega)]^\dagger$. These components give access to spectral properties such as the local (A_i) or total (D) density-of-states (LDOS)

$$A_i(\omega) = \text{i} [G_{ii}^>(\omega) - G_{ii}^<(\omega)], \quad D(\omega) = \sum_i A_i(\omega). \quad (6)$$

Correlation effects are included in Eq. 1 via the self-energy $\Sigma^{\text{R/A}}(\omega)$ which contains the time-diagonal Hartree–Fock (HF) self-energy as well as the time non-local correlation part, e.g. the second Born (2B) or GW approximation. The mean-field (Hartree-Fock) contribution

can be included into the single-particle Hamiltonian \hat{h}^{eff} that replaces Eq. (3),

$$\hat{h}^{\text{eff}} = -J \sum_{\langle i,j \rangle, \alpha} \hat{c}_{i\alpha}^\dagger \hat{c}_{j\alpha} + U \sum_i (n_{i,\uparrow} \hat{n}_{i,\downarrow} + n_{i,\downarrow} \hat{n}_{i,\uparrow}), \quad (7)$$

with $\hat{n}_{i,\alpha} = \hat{c}_{i\alpha}^\dagger \hat{c}_{i\alpha}$ and $n_{i,\alpha} = \langle \hat{n}_{i,\alpha} \rangle$.

The determination of the GW self-energy is more demanding and takes several steps. First, the retarded polarizability $\mathbf{P}^{\text{R}}(\omega)$ has to be calculated. It is advantageous to do this in time space where $\mathbf{P}^{\text{R}}(t)$ in the random-phase approximation (RPA) is defined as a simple product of time-local Green functions:

$$\mathbf{P}^{\text{R}}(t) = -i\hbar\Theta(t) \{ \mathbf{G}^>(t) \circ [\mathbf{G}^<(t)]^* - \mathbf{G}^<(t) \circ [\mathbf{G}^>(t)]^* \}. \quad (8)$$

Here, $\Theta(t)$ is the Heaviside step function, \circ denotes the Hadamard product between matrices, and the $\mathbf{G}^{\gtrless}(t)$ are determined by Fourier transform,

$$\mathbf{G}^{\gtrless}(t) = \mathcal{F} [\mathbf{G}^{\gtrless}(\omega)] := \frac{1}{2\pi} \int_{-\infty}^{\infty} d\omega e^{-i\omega t} \mathbf{G}^{\gtrless}(\omega). \quad (9)$$

The polarizability in Eq. 8 as introduced by Hedin³ becomes equivalent to the familiar Lindhard formula⁴ when considering non-interacting particles. Using the polarizability the retarded component of the (non-singular) dynamically screened interaction $\mathbf{W}^{\text{R}}(\omega)$ can be determined. It is defined as the full dynamically screened potential minus the bare interaction and obeys a Dyson equation as the Green function [cf. Eq. (1)],

$$\mathbf{W}^{\text{R}}(\omega) = U^2 \mathbf{P}^{\text{R}}(\omega) + U^2 [\mathbf{P}^{\text{R}}(\omega)]^2 \mathbf{W}^{\text{R}}(\omega), \quad (10)$$

where again a Fourier transform $\mathbf{P}^{\text{R}}(\omega) = \mathcal{F} [\mathbf{P}^{\text{R}}(t)]$ is used. The solution of Eq. (10) is given by

$$\mathbf{W}^{\text{R}}(\omega) = [\mathbf{1} - U^2 [\mathbf{P}^{\text{R}}(\omega)]^2]^{-1} U^2 \mathbf{P}^{\text{R}}(\omega). \quad (11)$$

In the Hubbard model every other term of the screened interaction (the terms with an even number of bubbles in the diagrammatic picture) vanishes due to the on-site interaction and Pauli blocking resulting in the rather unusual form of Eqs. 10 and 11.

The lesser and greater components of the screened interaction can be calculated using

$$\mathbf{W}^<(\omega) = f_{\text{B}}(\omega - \mu) [\mathbf{W}^{\text{R}}(\omega) - \mathbf{W}^{\text{A}}(\omega)], \quad (12)$$

$$\mathbf{W}^>(\omega) = (f_{\text{B}}(\omega - \mu) + 1) [\mathbf{W}^{\text{R}}(\omega) - \mathbf{W}^{\text{A}}(\omega)], \quad (13)$$

with the Bose distribution $f_{\text{B}}(\omega) = 1/(e^{\beta\omega} - 1)$ and $\mathbf{W}^{\text{A}}(\omega) = [\mathbf{W}^{\text{R}}(\omega)]^\dagger$. In the next step the self-energy can be calculated. Again, doing so in time space is advantageous due to time-local relations. First, the lesser and greater components are given by

$$\boldsymbol{\Sigma}^{\geq}(t) = i\hbar \mathbf{W}^{\geq}(t) \circ \mathbf{G}^{\geq}(t), \quad (14)$$

where $\mathbf{W}^{\geq}(t) = \mathcal{F} [\mathbf{W}^{\geq}(\omega)]$ was used. The retarded component is defined as

$$\boldsymbol{\Sigma}^{\text{R}}(t) = \Theta(t) [\boldsymbol{\Sigma}^>(t) - \boldsymbol{\Sigma}^<(t)], \quad (15)$$

and with the Fourier transform $\boldsymbol{\Sigma}^{\text{R}}(\omega) = \mathcal{F} [\boldsymbol{\Sigma}^{\text{R}}(t)]$ the self-energy in *GW* approximation can be included in Eq. (1).

For the self-consistent solution of Eq. (1) the following scheme is iterated until convergence is achieved:

- 0) Diagonalize the effective single-particle Hamiltonian \hat{h}^{eff} , cf. Eq. (7), and initialize $\mathbf{G}^{\text{R}}(\omega) = \mathbf{G}_0^{\text{R}}(\omega)$, cf. Eq. (2)
- 1) Calculate $\mathbf{G}^{\geq}(\omega)$ from $\mathbf{G}^{\text{R}}(\omega)$, using Eqs. (5) and (4)
- 2) Perform the Fourier transform, $\mathbf{G}^{\geq}(t) = \mathcal{F} [\mathbf{G}^{\geq}(\omega)]$
- 3) Calculate $\boldsymbol{\Sigma}^{\geq}(t)$ and $\boldsymbol{\Sigma}^{\text{R}}(t)$ using Eqs. (8)–(15)

- 4) Perform the Fourier transform $\Sigma^{\text{R}}(\omega) = \mathcal{F} [\Sigma^{\text{R}}(t)]$
- 5) Solve the Dyson equation for $\mathbf{G}^{\text{R}}(\omega)$, Eq. (1), using the new $\Sigma^{\text{R}}(\omega)$
- 6) If $\mathbf{G}^{\text{R}}(\omega)$ is not yet converged start again at 1)

To improve the convergence of the above scheme, the input Green function at iteration N ($\mathbf{G}_{\text{in},N}^{\text{R}}$) is determined by mixing the solutions of the two previous iterations

$$\mathbf{G}_{\text{in},N}^{\text{R}}(\omega) = \alpha \mathbf{G}_{\text{out},N-1}^{\text{R}}(\omega) + (1 - \alpha) \mathbf{G}_{\text{out},N-2}^{\text{R}}(\omega), \quad (16)$$

where a mixing parameter of $\alpha = 0.05$ was used.

While throughout this work the above presented scheme is solved self-consistently, there exists an alternative approach, G_0W_0 , where only one iteration is performed. We compared both strategies and found that, while overall the results were qualitatively comparable, the self-consistent solution better describes screening effects, e.g. the spatial extension of the zero-energy state discussed in Fig. 1 of the main text and Fig. S2.

To generate the spatially resolved dI/dV data $2p_z$ orbitals are placed on top of the atomic sites of the lattice structure, following the procedures described in Refs. 5,6. In a first approximation the differential conductance in the energy interval $[E_1, E_2]$ at a constant height z_0 above the system is then given by

$$\frac{dI}{dV}(x, y, z_0) = \int_{E_1}^{E_2} d\omega \sum_{ij} A_{ij}(\omega) z_0^2 e^{\lambda^{-1}|\mathbf{r}-\mathbf{r}_i|} e^{\lambda^{-1}|\mathbf{r}-\mathbf{r}_j|}, \quad (17)$$

with $z_0 = 4\text{\AA}$, $\lambda = 1.72\text{\AA}$, and

$$A_{ij}(\omega) = i [G_{ij}^>(\omega) - G_{ij}^<(\omega)]. \quad (18)$$

Determining the Hubbard interaction U for GW

The Hubbard Hamiltonian [Eq. (1) in the main text] includes two free parameters, the hopping amplitude $J = 2.7 \text{ eV}$ and the on-site interaction strength U . To obtain the value of U that is appropriate for use with the GW approximation, we perform calculations for a 7-9-AGNR heterostructure of six unit cells for various interaction strengths $U = 0, \dots, 3.5J$ and compare the band gap between the topological bulk bands to the experimental result of Ref. 8. The results are shown in Fig. S1. Increasing the interaction strength results in an opening of the band gap. We find that for $U = 2.5J$ the theory best reproduces the experimental band gap for the GNR heterostructure on Au(111). Therefore, this choice of U includes screening effects of the metallic substrate which reduce the effective on-site interaction. For the description of free-standing GNRs a larger on-site interaction is required.⁹

Including environmental screening by modifying the Hubbard interaction U corresponds to assuming a constant dielectric function of the substrate ε_{env} which modifies the screened interaction of the isolated system $\mathbf{W}_{\text{iso}}^{\text{R}}$:

$$\mathbf{W}_{\text{tot}}^{\text{R}}(\omega) = \varepsilon_{\text{env}}^{-1} \mathbf{W}_{\text{iso}}^{\text{R}}(\omega). \quad (19)$$

In leading order the non-singular screened interaction in the Hubbard model is given by $\mathbf{W}_{\text{iso}}^{\text{R}}(\omega) = U_{\text{iso}}^2 \mathbf{P}^{\text{R}}(\omega)$, which corresponds to the well known static second Born approximation.

In our model, instead of using an external dielectric function, we include the substrate screening in an effective Hubbard interaction resulting in $\mathbf{W}_{\text{tot}}^{\text{R}}(\omega) = U_{\text{eff}}^2 \mathbf{P}^{\text{R}}(\omega)$. Comparing the above equations leads to

$$\varepsilon_{\text{env}}^{-1} U_{\text{iso}}^2 \mathbf{P}(\omega) = U_{\text{eff}}^2 \mathbf{P}(\omega), \quad (20)$$

which results in a relation between the Hubbard interaction of the isolated system, the

effective interaction, and the dielectric constant of the substrate,

$$U_{\text{eff}} = \frac{U_{\text{iso}}}{\sqrt{\varepsilon_{\text{env}}}}. \quad (21)$$

For similar systems separate fits for U_{eff} and U_{iso} lead to reasonable values for ε_{env} in the range of 2–5 for the Au(111) substrate.⁹ As a major advantage this approach does not violate any sum rules or conservation laws but preserves all properties inherent in the *GW* approximation. In general, this is not necessarily the case when considering more advanced (momentum or frequency dependent) external dielectric functions of the substrate.

Screening of topological states

The *GW* approximation reduces the spatial extension of the topological zero-energy end state. This is shown in Fig. S2 where the dI/dV maps of the zero-energy state of a 7-9-AGNR heterostructure containing six unit cells are compared for TB and *GW*. While the state is strongly confined in the end cell for *GW*, for TB it extends well into the second and third unit cell. This gives rise to the unphysical contribution at the Fermi energy observed in Fig. 1(b) of the main text for TB.

7-AGNR states

To classify the states occurring for the extended system in Fig. 4(b) in the main text, in Fig. S3 the DOS and the dI/dV maps of three states are shown for a pristine 7-AGNR system containing 504 atoms for *GW*. The states are labeled “1, 3 and 5”, for a better comparison to the corresponding states in Fig. 4(b) of the main text. While the energy levels slightly differ, the spatial distribution of the pristine 7-AGNR states perfectly agrees with the states localized in the short 7-AGNR regions of the extended 7-9-AGNR.

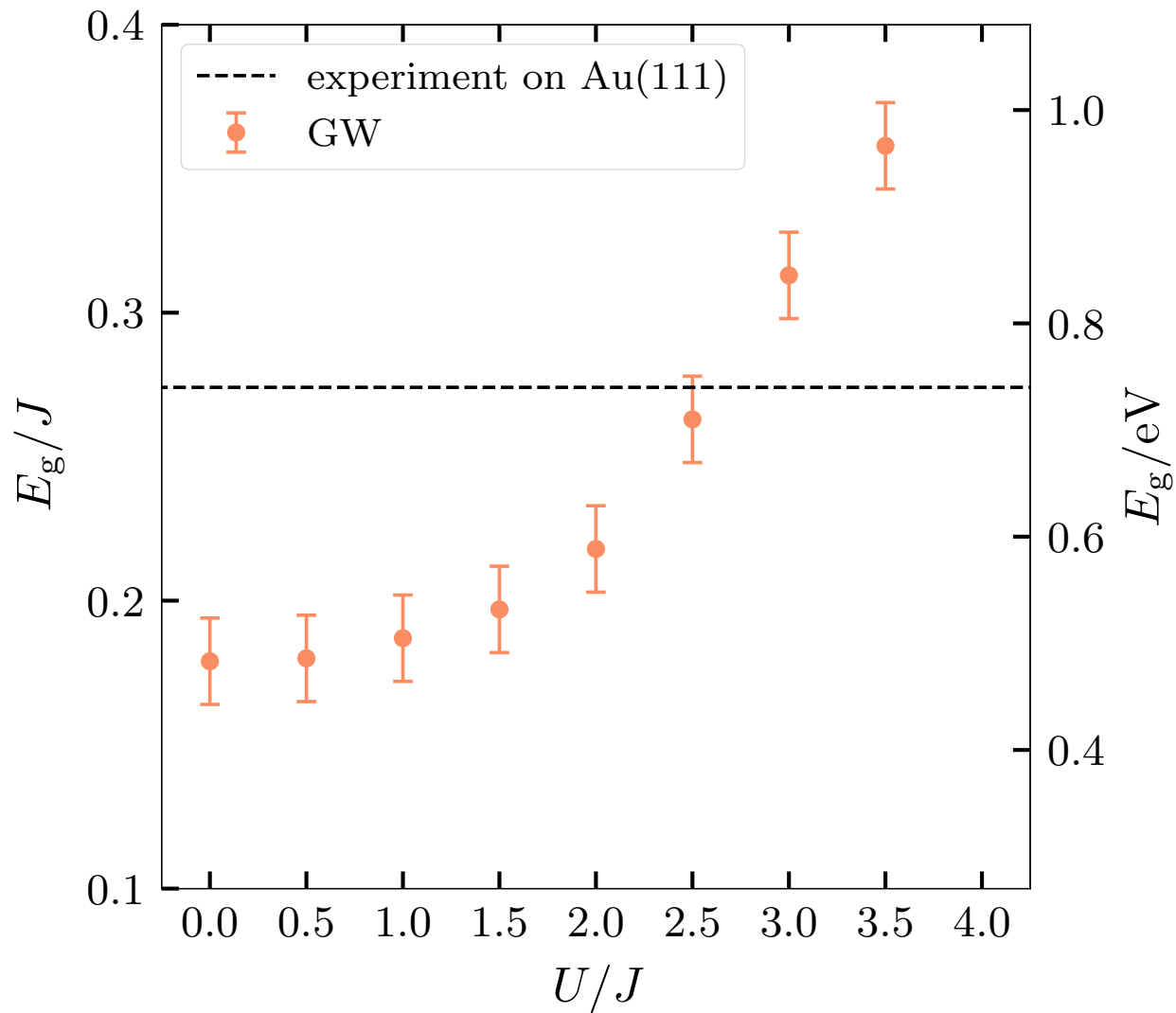


Figure S1: Gap between the topological bulk bands of a 7-9-AGNR heterostructure containing six unit cells, calculated using the *GW* self-energy (see text) and different interaction strengths, $U = 0, \dots, 3.5J$. The dashed line marks the experimental value for the same heterostructure on Au(111) obtained in Ref. 8.

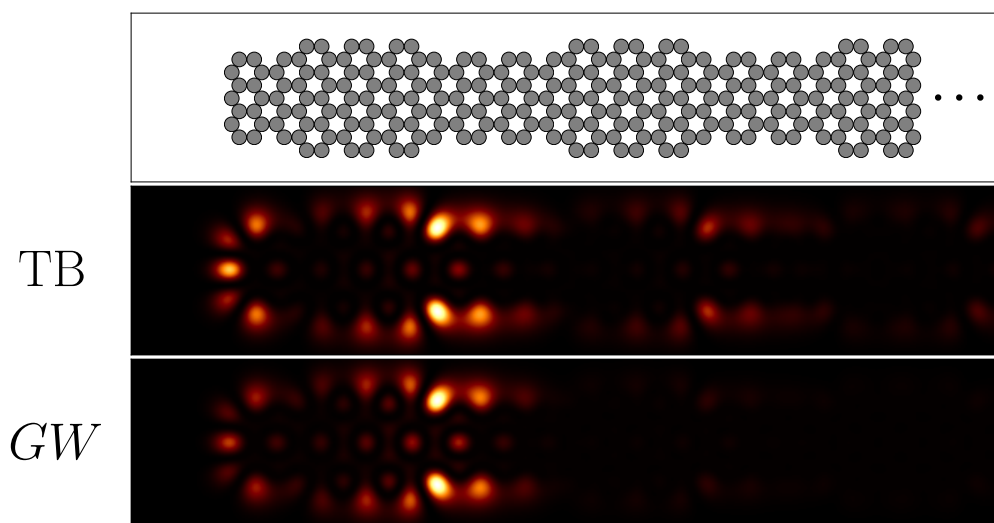


Figure S2: Differential conductance map of the zero-energy state of a 7-9-AGNR heterostructure containing six unit cells, from TB and GW simulations. Only part of the system is shown as indicated by the black dots.

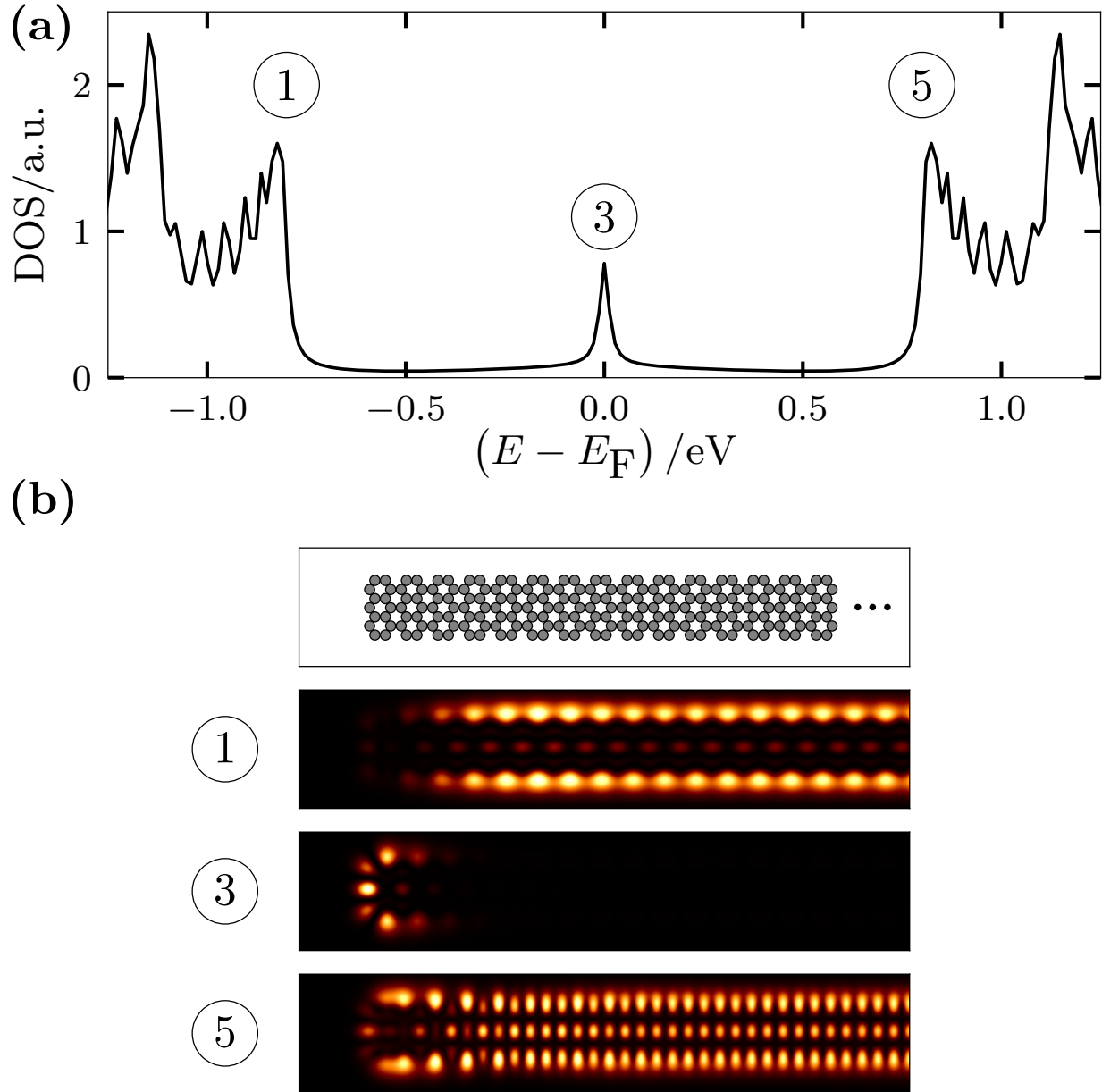


Figure S3: (a) DOS for a pristine 7-AGNR containing 504 atoms within the *GW* self-energy. (b) Differential conductance maps for the three states labeled in (a). Only part of the system is shown as indicated by the black dots.

References

- (1) Essler, F. H.; Frahm, H.; Göhmann, F.; Klümper, A.; Korepin, V. E. *The one-dimensional Hubbard model*; Cambridge University Press: Cambridge, 2005.
- (2) Schlünzen, N.; Joost, J.-P.; Heidrich-Meisner, F.; Bonitz, M. Nonequilibrium dynamics in the one-dimensional Fermi-Hubbard model: Comparison of the nonequilibrium Green-functions approach and the density matrix renormalization group method. *Physical Review B* **2017**, *95*, 165139.
- (3) Hedin, L. New Method for Calculating the One-Particle Green's Function with Application to the Electron-Gas Problem. *Phys. Rev.* **1965**, *139*, A796–A823.
- (4) Onida, G.; Reining, L.; Rubio, A. Electronic excitations: density-functional versus many-body Green's-function approaches. *Rev. Mod. Phys.* **2002**, *74*, 601–659.
- (5) Tersoff, J.; Hamann, D. R. Theory of the scanning tunneling microscope. *Phys. Rev. B* **1985**, *31*, 805–813.
- (6) Meunier, V.; Lambin, P. Tight-Binding Computation of the STM Image of Carbon Nanotubes. *Phys. Rev. Lett.* **1998**, *81*, 5588–5591.
- (7) Reich, S.; Maultzsch, J.; Thomsen, C.; Ordejón, P. Tight-binding description of graphene. *Phys. Rev. B* **2002**, *66*, 035412.
- (8) Rizzo, D. J.; Veber, G.; Cao, T.; Bronner, C.; Chen, T.; Zhao, F.; Rodriguez, H.; Louie, S. G.; Crommie, M. F.; Fischer, F. R. Topological band engineering of graphene nanoribbons. *Nature* **2018**, *560*, 204.
- (9) Joost, J.-P.; Schlünzen, N.; Bonitz, M. Femtosecond Electron Dynamics in Graphene Nanoribbons – A Nonequilibrium Green Functions Approach Within an Extended Hubbard Model. *Phys. Status Solidi B* **2019**, *256*, 1800498.